Ferroelectric structure of $KNbO_3$ and $KTaO_3$ from first-principles calculations

A. V. Postnikov,* T. Neumann, and G. Borstel
Universität Osnabrück-Fachbereich Physik, D-49069 Osnabrück, Germany

M. Methfessel
Institut für Halbleiterphysik, P.O. Box 409, D-15204 Frankfurt an der Oder, Germany
(Received 28 April 1993)

Based on the results of total-energy calculations using the full-potential linear muffin-tin orbital method, the equilibrium ground-state structure is determined in perovskite-type $KNbO_3$ and $KTaO_3$ complex oxides. The first compound is found to have a ferroelectric zero-temperature ground state, induced by atomic displacements along [111], as is consistent with the experimentally determined low-temperature crystal structure. The displacements along [001] give rise to another ferroelectric structure which is stable in the constrained tetragonal symmetry; this structure, however, corresponds to a saddle point on a more general path connecting two adjacent [111]-type displacements. $KTaO_3$ was found to be stable in the undistorted cubic phase at zero temperature, exhibiting a soft phonon mode, but it can be driven to a ferroelectric state by negative pressure.

I. INTRODUCTION

The ferroelectricity in oxidic crystals is generally understood as being due to a balance of long-range Coulomb repulsion and short-range chemical bonding. For many systems there is, however, a controversy concerning the mechanism by which the ferroelectric ordering is established—whether it is an order-disorder transition or a displacive transition, involving freezing out of a particular optical-phonon mode, as predicted by the Cochran theory.[1]

Particularly for $KNbO_3$ this controversy is not yet definitely resolved; experimental evidence in favor of soft-mode damping[2,3] as well as of an order-disorder[4,5] character of the ferroelectric transition has been presented.

Whatever the ferroelectricity-driving mechanism, the low-temperature ground state of a ferroelectric crystal is ordered and thus can be subject to a band-structure calculation, aimed at the optimization of the unit-cell geometry and the extraction of some energy-related parameters (such as the shape and the width of the potential well related to a ferroelectric distortion), which may be further fitted into more sophisticated theoretical models of disordering and alloying.

The first-principles calculations which can really give some insight into the microscopic interactions and hybridization-dependent balance of driving forces for a ferroelectric transition have become feasible only recently, as sufficiently fast band-structure calculation methods which put essentially no restriction onto the shape of the potential and charge density have been developed. Calculations of this kind for perovskite-type oxides ($BaTiO_3$ and $SrTiO_3$) have been performed by Weyrich and Siems,[6,7] followed by an extensive study on the lattice dynamics in $BaTiO_3$ by Cohen and Krakauer[8] (see also Ref. 9). The full-potential calculation minimizing total energy versus tilting and breathing distortions of oxygen octahedra in another perovskite-type oxide, $BaBiO_3$, has been performed in Ref. 10. Finally, a full-potential calculation by the full-potential linearized-augmented-plane-wave method has been reported recently for $KNbO_3$.[11] This paper was essentially aimed at the evaluation of the macroscopic polarization in the experimentally known crystal structure of the tetragonal phase, and no search for the lowest-energy ground-state structure has been done there.

In the present paper, we look for the crystal structures which minimize the total energy of $KNbO_3$ and $KTaO_3$ crystals, under the constraint that the distortions from the paraelectric cubic phase occur either in rhombohedral or in tetragonal symmetry, with one formula unit per ferroelectric unit cell. As is experimentally known, the first of the compounds in question exhibits the same sequence of phase transformations on cooling as $BaTiO_3$ (i.e., from cubic to tetragonal to orthorhombic to rhombohedral[12]); the second one remains in the cubic non-ferroelectric phase down to lowest temperatures. However, $KTaO_3$ is very close to the ferroelectrical threshold, as follows from the existence of soft phonon mode at $\mathbf{q} = \mathbf{0}$. Actually, as we show in this paper, $KTaO_3$ could be driven into a ferroelectric state by slight expansion of its crystal lattice. $KNbO_3$ and $KTaO_3$ form an unrestricted solid solution (KTN), the dielectric properties of which can be conveniently adjusted by the concentration. The doped crystals based on KTN have promising applications as optically active media, and the present study of the microscopic structure of the pure constituents is the necessary first step in a theoretical understanding of the properties of this group of materials.

The paper is organized as follows: In Sec. II, we introduce the necessarily simplifying assumption for the

microscopical structure of the ferroelectric phase. In Sec. III, the calculation setup, including the choice of the basis set, is discussed. In Sec. IV, the equilibrium volumes and other bulk properties for the cubic phase of the systems in question are calculated. In Sec. V, results of the total-energy calculations for $KNbO_3$ are summarized for two ferroelectric phases and different cell volumes. In Sec. VI, the tendency towards ferroelectric instability is discussed for $KTaO_3$.

II. CHOICE OF THE STRUCTURAL MODELS

The primary objective of our study was to simulate, based on the results of calculations, the correct low-temperature ferroelectric ground state of $KNbO_3$ and to understand why the ferroelectric transition does not occur in the isostructural compound $KTaO_3$. Although we did not use any experimentally determined parameters in our calculation, the use of some previous empirical knowledge helped to minimize the necessary computational effort, imposing several experimentally well-justified constraints which reduced the number of independent structure-defining variables.

Thus, we assumed that the Bravais lattice of $KNbO_3$, as well as that of $KTaO_3$, remain cubic at lowest temperatures, although the displacements of atoms lower the space group from $Pm3m$ above the Curie temperature to $R3m$ below the last structure transition. Indeed, the experimentally determined $\alpha = \beta = \gamma$ angles of the rhombohedral unit cell differ from 90° by merely 11′;[13] according to the calculations of Ref. 8 for $BaTiO_3$, the effect of such small rhombohedral strain on the total energy is negligible.

On the other hand, the [001] strain which is known to be as large as $(c - a)/a = 1.65\%$ in the tetragonal ferroelectric phase,[12] cannot be as safely neglected in the total-energy calculations. Indeed, the tetrahedral strain included in the calculations for $BaTiO_3$ (Ref. 8) has been shown to lower the total-energy at fixed atomic displacements by the same order of magnitude as the net atomic displacements do in the absence of strain. Therefore, when considering the tetrahedral ferroelectric phase, we preferred to study the combined effect of atomic displacements and strain on the total-energy surface.

Another assumption was that all oxygen atoms undergoing ferroelectric displacements are shifted as a rigid sublattice. This is, in principle, justified only within 5% accuracy—of this size is the difference of displacements of inequivalent oxygen atoms along [001] in the tetragonal phase, as well as the difference of individual oxygen atom displacements along [100] and [001] in the rhombohedral phase.[12] However, these expected deformations are known to be substantially smaller than the differences between the displacements of O and K atoms.

Therefore, the atomic positions of the ferroelectric phases we studied were defined by just two parameters within the given space group, namely, by the relative displacements of the potassium atom and of the rigid oxygen cage either along [111] (in the rhombohedral lattice) or along [001] (in the tetragonal lattice, combined also with tetragonal strain) in the coordinate system related to fixed Nb (or Ta) atoms. For each space group corresponding to one or another ferroelectric phase, the total energy was then mapped as a function of these two parameters and the equilibrium geometry found from the global total-energy minimum.

The orthorhombic ferroelectric phase, which is, as experimentally known, an intermediate one existing in the temperature range above the rhombohedral and below the tetragonal phases of $KNbO_3$, has not been considered in the present study, because its more complicated crystal structure with two formula units per unit cell demands more computational effort. However, full-potential calculations for orthorhombic structure, if performed, would be possibly crucial for a better understanding of the structural mechanism behind the observed sequence of ferroelectric phase transitions.

III. TECHNICAL ASPECTS OF CALCULATION

The calculations for perovskite-type $KNbO_3$ and $KTaO_3$ were performed by the full-potential linear muffin-tin orbital (LMTO) method.[14,15] As is customary for an LMTO approach, the basis for the wave function consists of atom-centered Hankel functions which are augmented by numerical solutions of the radial Schrödinger equation within atomic spheres. In our case the atomic spheres are nonoverlapping. The output charge density as well as the product of two LMTO's (needed for constructing the Hamiltonian matrix) are represented in the interstitial region by fitting a linear combination of Hankel functions to the values and slopes on the sphere boundaries.

The interstitial exchange-correlation quantities are treated in the same way. This procedure makes it possible to evaluate the involved integrations over the interstitial region with small effort, leading to a high computational effectiveness. This method has been successfully applied to the study of a variety of compounds, including (among nonmetallic systems) simple oxides[16] and doped perovskite $BaBiO_3$.[10]

In order to provide sufficient variational freedom, it is essential in the calculation method we used to extend the basis by using LMTO's with various localizations. The envelope function decays as $e^{-\kappa r}$, where $-\kappa^2$ is the kinetic energy of the Hankel function envelope.

The choice of the basis set we found to be optimal for describing the valence band of the systems in question is presented in Table I. Apart from the states listed there, Nb 4s and Ta 5s have been explicitly included in the semicore panel, substituting correspondingly Nb 5s

TABLE I. Basis set and MT-sphere radii used in the calculation.

Atom	$\kappa_1^2 = -0.01$ Ry	$\kappa_2^2 = -1.0$ Ry	$\kappa_3^2 = -2.3$ Ry	R_{MT} (a.u.)
K	4s 3p 3d	4s 3p		3.35
Nb	5s 4p 4d	5s 4p 4d	5s	1.85
Ta	6s 5p 5d 4f	6s 5p 5d	6s 5p	1.85
O	2s 2p 3d	2s 2p	2s 2p	1.55

and Ta 6s (the size of the secular equation matrix in the semicore panel has been kept the same as for the valence band). The effect of further expanding the basis on the final results (trends in the total energy as function of volume and atomic displacements) has been tested and found to be insignificant.

Our choice of the basis is based on the following considerations. The K 3p state, which gives rise to a quite narrow band in the gap between O 2s- and O 2p-originating bands,[17] exhibits nevertheless a considerable admixture to other valence-band states and therefore should not be treated as a semicore state. Even more unexpectedly, Nb 4p (and Ta 5p) states, which lie about 1 Ry below the O 2s band, are not well enough localized and participate in the hybridization with other states forming the valence band. This latest observation is consistent with the experience of Ref. 6, where in the calculation of $SrTiO_3$ and $BaTiO_3$ compounds (isostructural to ours) Ti 3p electrons were included in the band calculation, in order to ensure that the remaining Ti core fits into the atomic sphere. The K 3s state, which is situated in the energy scale some 0.3 Ry above the Nb 4p band, is, on the contrary, very well localized within the MT sphere of appropriate size, so that it may be safely treated as a true core state. Finally, Nb 4s (Ta 5s) is a typical low-lying semicore, and this is the only state which belongs to the semicore panel in our calculation.

This division of the participating electronic states into valence-band ones, semicore and "true core," is not obvious, but it is based on a thoroughful analysis of the degree of localization of various states and their contribution to the hybridization within the valence band. Any other choice does not affect the band structure considerably, but leads to an underestimation of the equilibrium volume (when the total energy is calculated as a function of the lattice constant). A neglect of the semicore contribution to the pressure may reduce the calculated equilibrium volume by 15–20 %. This happens in $KNbO_3$, if the Nb 4s state is treated as core or Nb 4p (or K 3p) as semicore (the same is true with respect to Ta 5s and Ta5p in $KTaO_3$).

It was not technically possible in the present-day version of the computer code we used to include more than one state with the same orbital momentum per atom in the valence band (as is typically the case in many other LMTO-based algorithms as well). Within the setup discussed above, any high-lying K 4p and Nb 5p (correspondingly Ta 6p) character was completely ignored in our calculation. Although this shortcoming is primarily expected to affect the description of the empty states in the conduction band and not those in the valence band contributing to the total energy, the possible effect of hybridization with the mentioned upper states deserves a special study in the future. As was emphasized in Ref. 18, the simultaneous treatment of Ti 3p and 4p states is essential for producing reasonable estimations of the electric-field gradient in titanium oxide. Apparently (as follows from our results discussed below) a similar demand is not crucial for the correct description of the ferroelectric ground-state structures; however, some quantitative corrections may result from taking the hybridization with vacant p states into account.

With the basis set so chosen, the calculated band structure is essentially nonsensitive to the particular choice of the MT sphere radii and quite close to that calculated in Ref. 17 by the LMTO-atomic-sphere-approximation (ASA) method. The same applies to the total energy-on-volume dependence (see Sec. IV) which has the same shape and the position of the minimum within some limits of varying the MT radii. Much finer trends in the total energy as function of atomic displacements are, however, more strongly affected by the variations of the MT sphere sizes. Based on the spatial distribution of self-consistent charge density over the unit cell (Fig. 1), we preferred to use the set of radii as shown in Table I, which clearly attributes charge densities centered at different atoms to their corresponding spheres, leaving only relatively smooth variations of the charge density over the interstitial region.

Another minor source of uncertainty concerns the termination of the spherical harmonic expansions at some value L_{max} in the decomposition of the charge density in the interstitial region. In the ideal case, these sums should be fully converged, which in many other calculations performed with this formalism had occurred already at $L_{max}=4$ (see, e.g., Ref. 15). For $KNbO_3$ and $KTaO_3$, because of considerable low-symmetry variations of the potential over the interstitial, this termination was not sufficient for obtaining correct behavior of the total energy as function of symmetry-lowering atomic displacements, and L_{max} should be increased up to 5 or 6 on the K site and can be increased up to 5 on the Nb site. The charge density inside and around the oxygen sphere may be still sufficiently well described by $L_{max}=4$, but we used a probably excessive value of 5 in the present calculation. The calculated equilibrium ferroelectric displacements have been checked to be stable within these limits of varying L_{max}. It should be noted that the attempt to use bigger L_{max} values on all atoms, e.g., equal to 6, apart from being unnecessarily time consuming, can create additional problems with the quality of the fit in the interstitial region, because of the excessive number of coefficients to be determined. One possible way to solve the problem is by introducing some extra empty spheres in the unit cell, as has been proposed in Ref. 15 for open structures.

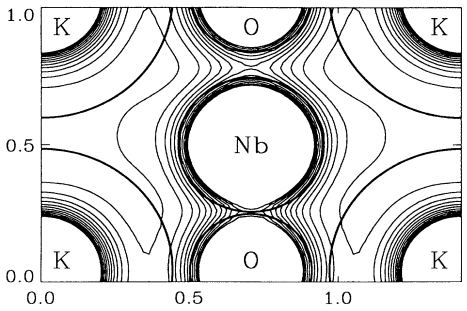

FIG. 1. Charge-density plot in the (110) plane of $KNbO_3$ with tetragonal displacement of Nb atom. The MT-sphere radii used in the calculation are indicated.

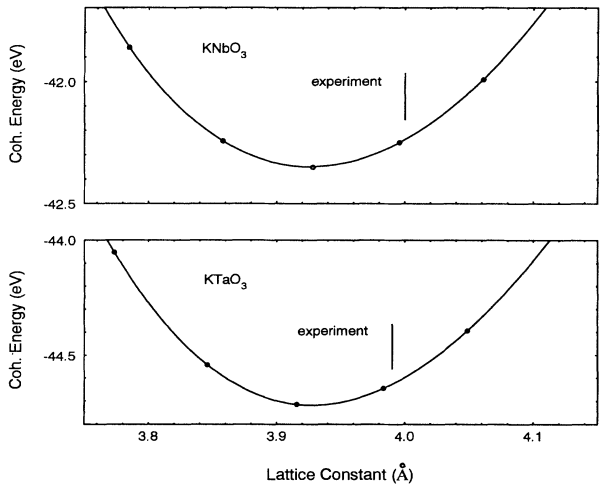

FIG. 2. Calculated total energy as function of the lattice constant for cubic $KNbO_3$ and $KTaO_3$. The experimental values of the lattice constants (extrapolated to zero temperature) are indicated by vertical labels.

The integrations in the reciprocal space have been well converged in the number of k points, which was found to happen starting from $8 \times 8 \times 8$ divisions of the full Brillouin zone, giving 40 k points in the irreducible wedge for the tetragonal structure and 60 for the rhombohedral structure.

IV. BULK PROPERTIES OF THE CUBIC PHASE

The calculated total energy as function of uniform volume expansion for the cubic phase of both systems is shown in Fig. 2. The vertical line for each compound denotes the lattice-constant value obtained from the extrapolation of experimentally measured volumes down to zero temperature. These values are 7.55 a.u. for $KNbO_3$ (basing on the unit cell volume data of Ref. 19) and 7.53 a.u. for $KTaO_3$.[20]

With the choice of the basis set as discussed above, the total energy calculated as a function of volume has the minimum at $V/V_0 = 0.95$ (for $KNbO_3$) and 0.96 (for $KTaO_3$). This $\sim -5\%$ difference in the evaluation of the equilibrium volume is typical for a calculation using the local-density approximation.

The values of the bulk moduli and cohesive energies as calculated from the energy–lattice-constant curve of Fig. 2 are listed in Table II. A comparison to earlier LMTO-ASA calculations[17] reveals a strong similarity. The only remarkable deviation found is that for the bulk modulus of $KNbO_3$, which is now closer to the experimental value. Lattice constants are underestimated by about 2%; the bulk modulus for $KTaO_3$ fits within the same quality to experimental data. The cohesive energy is again as in Ref. 17 overestimated by about 20%; however some uncertainty in the experimental determination of cohesive energy in Ref. 21 should be pointed out.

V. FERROELECTRIC GROUND STATE OF $KNbO_3$

A. Rhombohedral structure

In order to check if various atomic displacements may further lead to lowering the energy as the cubic symmetry gets broken, we mapped out the total energy as function of independent displacements of the K and O sublattices, with respect to Nb. This helps to visualize the directions of the "easiest" ferroelectric transformation and clarify the importance of "coupled" atomic displacements. The resulting total-energy map (calculated for the theoretical equilibrium cell volume, which is 95% of the experimental one) is shown in Fig. 3(a) and for the experimental volume in Fig. 3(b). The displacements are given in terms of the lattice constant for each volume. It is seen that in both figures, there is only one narrow total-energy valley which indicates the favorability of coupled K and O_6 displacements with respect to the Nb sublattice. There is only one pronounced minimum, which is shifted towards bigger displacements as the volume increases.

The position of equilibrium K and O displacements according to the experimentally determined low-temperature ferroelectric structure[12] is shown by a cross in Fig. 3. Our calculation therefore slightly underestimates the tendency of oxygen octahedra to displace and overestimates such tendency for the potassium atom. On the other hand, since the total-energy valley is essentially oriented along equal displacements of K and O, our calculation provides a support for a simplified assumption commonly cited (see, e.g., Refs. 4, 5, and 11) that the ferroelectric transition in cubic perovskites essentially involves the displacement of Nb (or, generally, of the B

TABLE II. Lattice constant a (Å), bulk modulus B (Mbar), and cohesive energy E_{coh} (eV/unit cell).

	a_{FP}	a_{ASA}	a_{expt}	B_{FP}	B_{ASA}	B_{expt}	E_{coh}^{FP}	E_{coh}^{ASA}	E_{coh}^{expt}
$KNbO_3$	3.93	3.94	$\sim$ 4.0[a]	2.08	2.47	$\sim$ 1.38[b]	-42.38	-42.19	-34.84[c]
$KTaO_3$	3.93	3.91	3.99[d]	2.25	2.25	2.30[e]	-44.72	-44.50	-28.84[c]
						2.20[f]			

[a] Reference 19, extrapolated value on $T = 0$ from lattice constants of the cubic high-temperature phase.
[b] Reference 21, calculated from cubic elastic constants.
[c] Reference 17.
[d] Reference 24.
[e] Reference 23, calculated from cubic elastic constants.
[f] Reference 25.

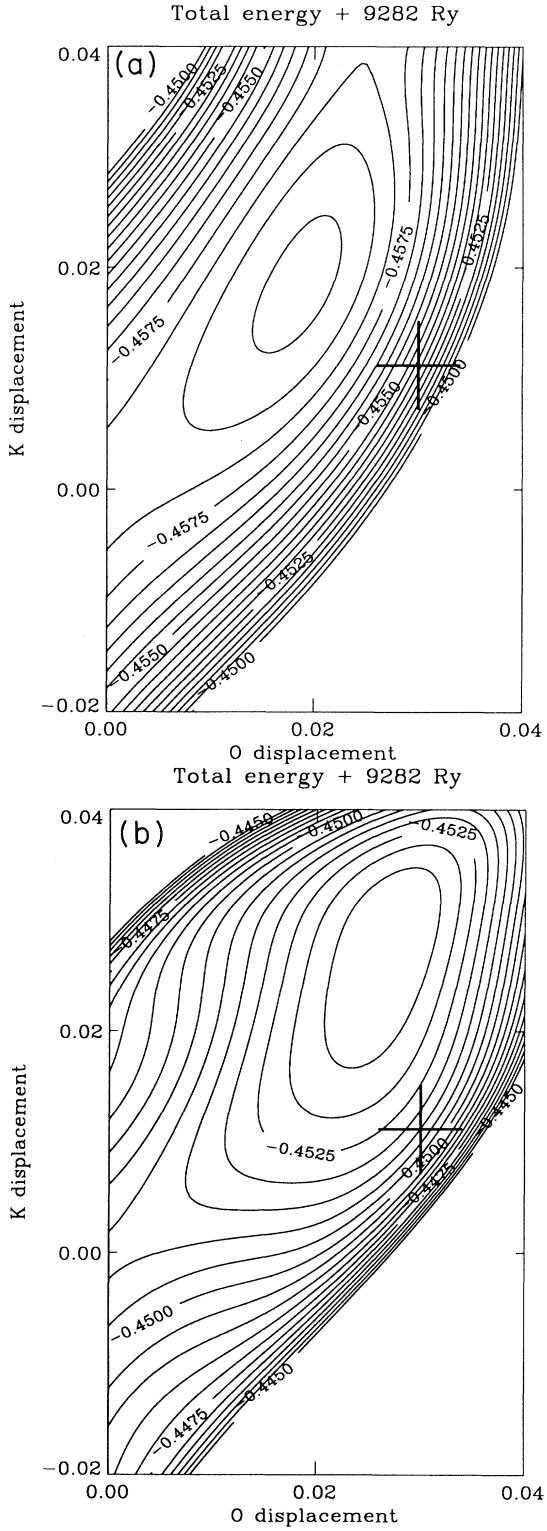

FIG. 3. Contour lines of the total energy over independent displacements of K and O along [111] in $KNbO_3$ for calculated equilibrium volume (a) and experimental volume (b). The experimentally determined displacement is indicated by a cross. Displacements are given in the units of the lattice constant, along all three crystallographic axes, i.e., $dX/a = dY/a = dZ/a$.

atom in the ABO_3 structure) with respect to the rigid lattice of all other atoms.

In order to study how stable the total-energy map is with respect to uniform volume changes and especially what it looks like at the experimental cell volume, we plotted the total-energy trends over individual "only-K" and "only-O_6" and combined "K+O_6" (i.e., "only-Nb") displacements for three different volumes (Fig. 4). One can see that the potential well of the K ion which is displaced in the rigid lattice of all other ions has an essentially parabolic shape and is the least sensitive to the variations of the cell volume. The potential well of the Nb ion would give rise to strongly anharmonic phonon properties at lower lattice volumes and triggers the ferroelectric transition already at $V = 90\%$ of the experimental volume, with the equilibrium displacement and the relative energy gain increasing with volume.

A suggested explanation of this behavior is the prononunced tendency of the Nb ion to form bonding states with at least three nearest oxygen atoms, shifting towards them along [111], as the size of the oxygen octahedron surrounding Nb increases. In Fig. 5, local densities of states at O and Nb sites are shown for the paraelectric cubic structure and for the rhombohedral structure, at the calculated equilibrium volume and (in the second case) for the relative Nb displacement as big as $dX = dY = dZ = 0.042a$, i.e., $0.073a$ along [111], in order to exaggerate the underlying trends. It is seen that the bonding peak at the bottom of the valence band which is formed by O $2p$ and Nb $4d$ states substantially grows as the ferroelectric displacement increases, thus giving the gain in the band energy. A similar observation has been made in Ref. 9, where the importance of Ti-O hybridization for the stability of the ferroelectric phase in $BaTiO_3$ was discussed. At even bigger Nb displacements, the gain in the band energy is overbalanced by short-range repulsion.

B. Tetragonal structure

Many of these observations are also applicable to tetrahedral displacements. That is, when K and O sublattices are allowed to be displaced independently along [001], the valley of the most effective energy lowering is situated along equal displacements of both. In other words, the ferroelectricity is mostly driven by the displacement of Nb atoms in an otherwise rigid lattice. The corresponding energy lowering is, as in the case of rhombohedral displacements, quite sensitive to the cell volume, so that our calculations performed at the theoretically determined (i.e., underestimated by 5%) volume gave a minimum only one-third as deep as that at the experimental volume, similarly to the situation shown in Fig. 4. The total energy as a function of [001] displacement of the Nb sublattice at the theoretical cell volume is shown in Fig. 6 (right panel). For comparison, the total energy as the function of net [111] displacement is reproduced in the left panel. The rhombohedral displacement results in a deeper total energy minimum; this is consistent with the fact that the low-temperature ferroelectric state of $KNbO_3$ has rhombohedral symmetry.

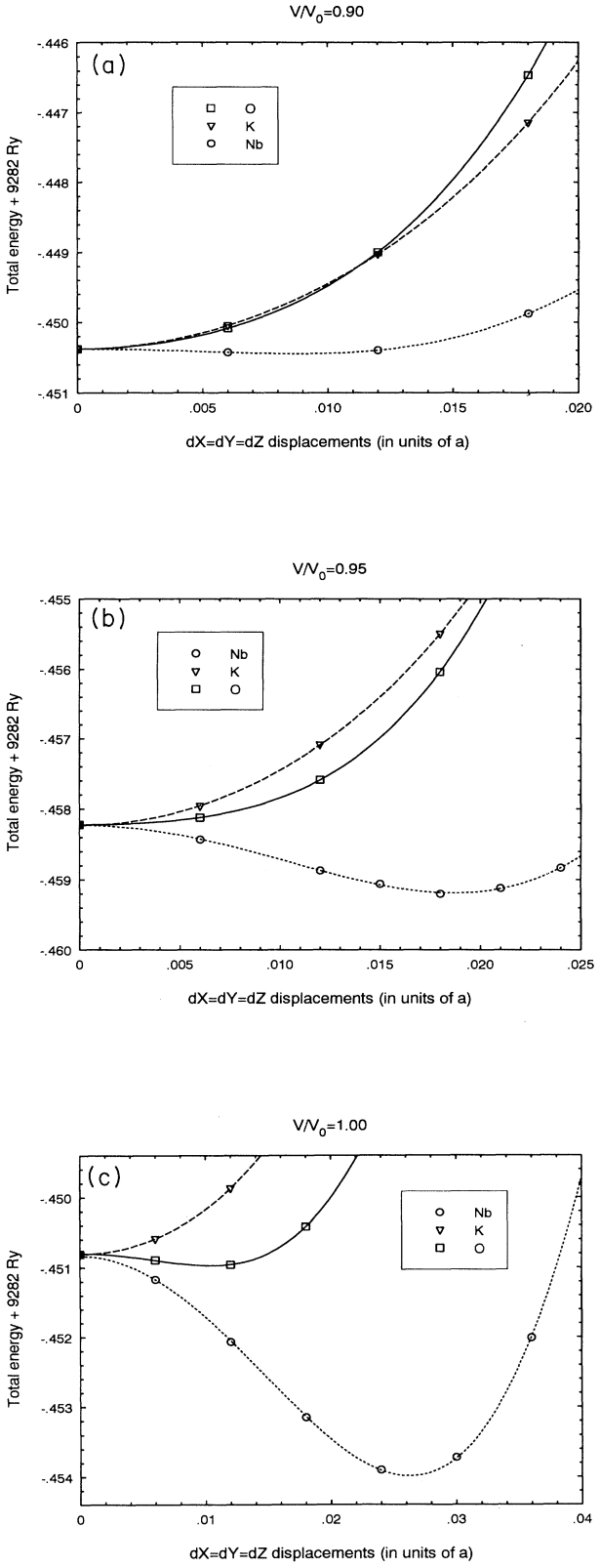

FIG. 4. Total energy versus rhombohedral displacement of K, Nb, and O atoms in the cubic unit cell of $KNbO_3$ for 90% of the experimental volume (a), calculated equilibrium volume (b), and the experimental volume (c).

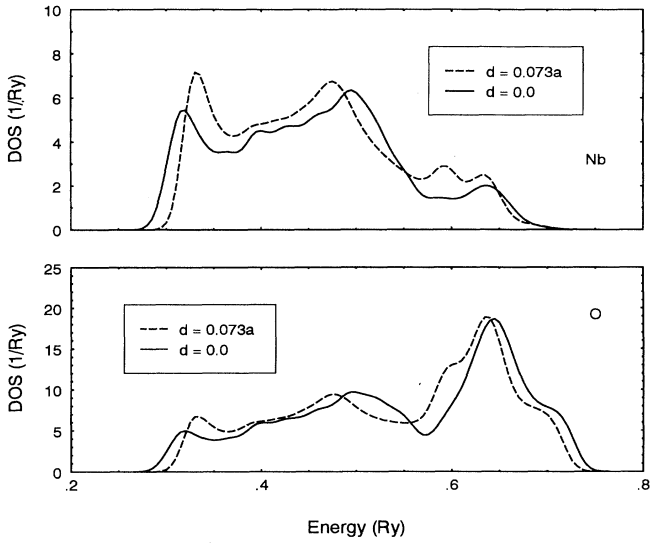

FIG. 5. Local densities of states at Nb site (top) and O site (bottom) in the rhombohedral unit cell (projected onto the muffin-tin spheres), with and without displacement of Nb by $0.072a$ along [111].

Since according to Ref. 8 the lattice strain may be an important contributor to the energy lowering at the tetrahedral ferroelectric transition in perovskites, we further studied its interplay with the Nb displacements. In Fig. 6, the total-energy dependence on the [001] Nb displacement for fixed strain of $(c-a)/a = 1.5\%$ is shown as the dashed line. It is seen that starting with a displacement of $0.02a$, the strain becomes energetically favorable and drives bigger atomic displacements than would be found in the unstrained lattice. In order to visualize the mutual effect of displacement and strain, the total-energy

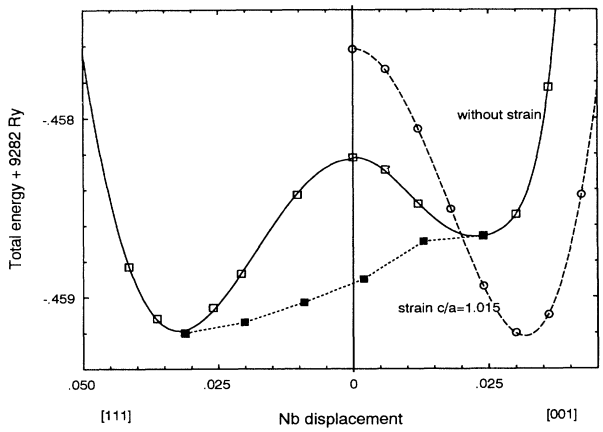

FIG. 6. Total energy versus rhombohedral displacement (left panel) and tetragonal displacement (right panel) of Nb in $KNbO_3$: solid line, for calculated equilibrium lattice constant without strain; dashed line, with tetragonal strain $c/a = 1.015$. The dotted line traces the calculated total-energy values at the equidistant points along the straight path from minimal-energy tetragonal to minimal-energy rhombohedral structure.

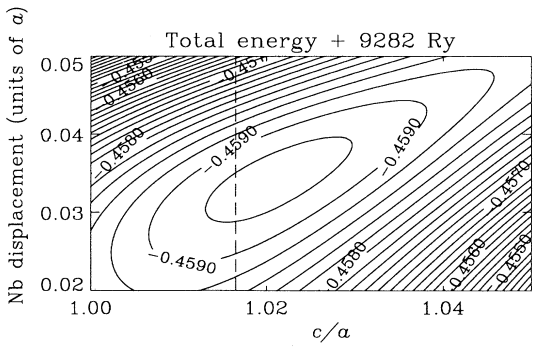

FIG. 7. Contour lines of the total energy over [001] displacements of Nb and tetragonal strain in $KNbO_3$. The experimental value of the experimental strain is indicated by the dotted line.

surface is shown in Fig. 7 as a function of these two variables. It is worth noting that the experimental value of tetrahedral strain in $KNbO_3$ (1.65%, dashed line in Fig. 7) is fairly well reproduced in the total-energy calculation.

Finally, we would like to establish some relation between the two lowest-energy structures which were found, the tetragonal and rhombohedral phases of $KNbO_3$. Of particular interest is the question of whether the tetragonal phase corresponds to a saddle point on the total-energy surface versus various Nb displacements, or whether there is a local energy minimum associated with this structure. If the former is true, then the observed tetragonal ferroelectric structure should be interpreted as a time average of the process of Nb atoms wandering over several [111]-directed potential wells, as supposed in the eight-site model.[4,5] In order to clarify this point, we traced the total energy along the straight-line path from the minimum in the rhombohedral structure to that of the tetragonal structure, performing a sequence of calculations on units cells with correspondingly reduced symmetry, but with a cubic Bravais lattice, i.e., ignoring the tetragonal strain. As can be seen from Fig. 6, these calculations reveal that the energy minimum of the tetragonal phase is indeed a saddle point, since symmetry-lowering displacements of Nb from this position along [110] uniformly reduce the total energy towards that of rhombohedral phase which is a true ground state.

The presence of tetragonal strain of course complicates the whole picture—the potential well related to a tetragonal distortion gets considerably deepened, and it is not obvious along which path the transition from rhombohedral to tetragonal ferroelectric structure may occur. As follows from the experimentally known sequence of ferroelectric phases in $KNbO_3$, such path would most probably incorporate the orthorombic phase, the analysis of which is beyond the scope of the present paper.

VI. VOLUME-DEPENDENT TENDENCY FOR FERROELECTRICITY IN $KTaO_3$

For $KTaO_3$, we performed a similar analysis of the total energy behavior under various displacements as for $KNbO_3$. As for the latter system, the combined displace-

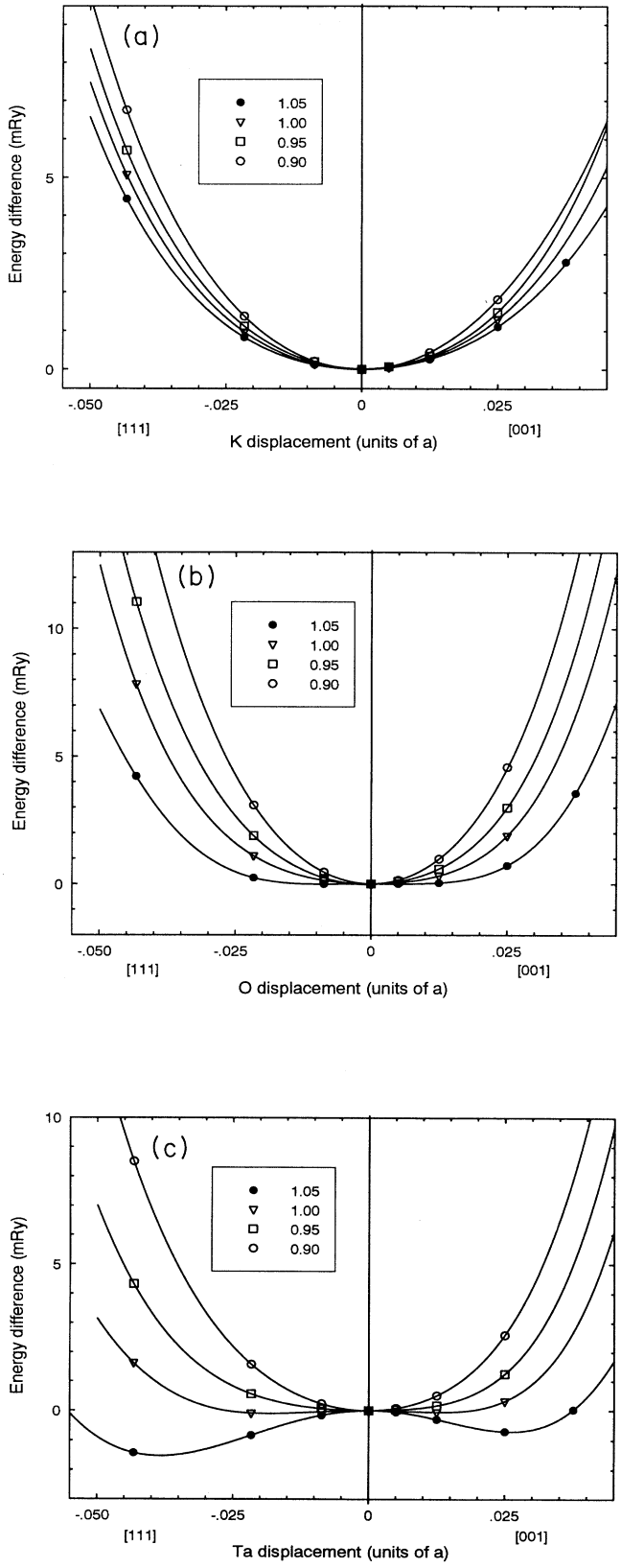

FIG. 8. Total energy versus rhombohedral (left panels) and tetragonal (right panels) displacements of K (a), O (b), and Ta (c) atoms in $KTaO_3$ for four different volumes.

ment of coupled K and O sublattices or, equivalently, the "only-Ta" displacements result in lower total energy than separate "only-K" and "only-O" displacements. However, the crucial difference from the case of $KNbO_3$ is that now (under the constraint of constant equilibrium volume) the cubic structure remains favored over all possible displaced structures.

The relative changes of the total energy with respect to that calculated for the cubic phase are, however, quite sensitive to the variations of volume. Generally, lattice compression stabilizes the cubic phase, whereas lattice expansion favors a ferroelectric instability. In Fig. 8, the set of total-energy curves over independent displacements of individual atoms along [111] and [001] is presented for a sequence of volumes.

The volume effect is least pronounced on the position of the K atom, which is situated in an almost spherically symmetric parabolic potential well [Fig. 8(a)]. For the O atoms (Fig. 8), the anharmonic contribution to their coupled movement is seen to increase considerably with volume, and the anisotropy of the related potential well with respect to [111] and [001] directions is now clearly seen. Finally, the displacement of Ta (Fig. 8) occurs in an even more anisotropic potential well, the shape of which apparently indicates considerable phonon frequency softening below the experimental volume as well as the tendency to go off center, forming a ferroelectric structure for larger volumes. Our calculation correctly predicts that the equilibrium ground-state structure, i.e., that corresponding to the calculated equilibrium volume, remains paraelectric in spite of the strong soft-mode instability. The fact that the crystal at experimental volume, according to calculation, is already slightly behind the ferroelectric threshold may possibly be revised in further studies; appropriately introduced corrections to the local-density functional result in a more exact estimate of the equilibrium volume for the system in question,[22] and the analysis of the quite sensitive behavior near the ferroelectric threshold should be, in principle, done on the same footing.

Some insight into the origin of the different tendencies towards the ferroelectric transition in $KNbO_3$ and $KTaO_3$ can be gained from the analysis of their densities of states in the valence band. In Fig. 9, contributions from Ta and O are shown for the same conditions as those from Nb and O in Fig. 5. The most noticeable difference to Fig. 5 is the absence of the evolution of the Ta–O bonding peak at the valence-band bottom under displacement. This is apparently due to the fact that because of the slightly bigger size of the Ta atom compared to Nb (as is revealed by the slightly bigger bandwidth of $KTaO_3$), the covalent part of the Ta–O bond is more saturated, and practically no energy gain results from the symmetry-breaking displacement of the Ta atom towards three of its neighbors in the O_6 cage. This view is consistent with the generally less ionic character of bonding in $KTaO_3$, as compared to $KNbO_3$.

VII. CONCLUSION

In the present paper, we studied the tendencies for the phase transition towards the ferroelectric structure

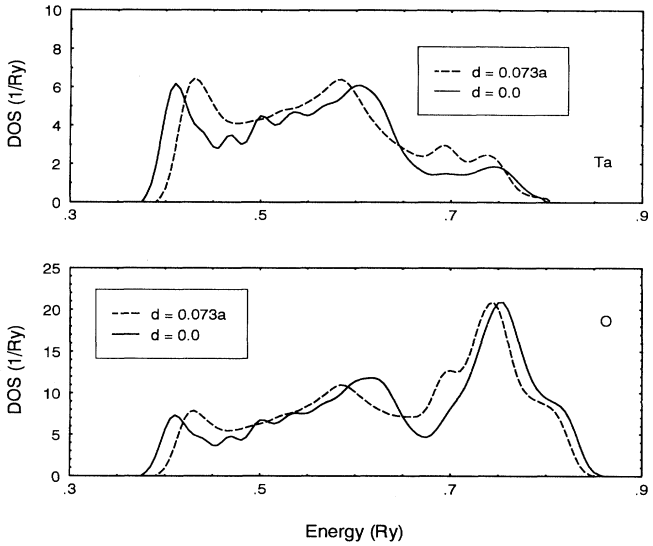

FIG. 9. Local densities of states at Ta site (top) and O site (bottom) in the rhombohedral unit cell; notation as in Fig. 5.

in $KNbO_3$ and $KTaO_3$ and have determined the ground-state crystal structures using full-potential LMTO calculation in the local-density approximation. The local-density approximation, which, as is well known, underestimates by several percent the equilibrium cell volume and hence (for the crystals considered) the tendency towards ferroelectric transition, provides, however, qualitatively correct results concerning the ground-state crystal structures. Thus, the lowest-energy ferroelectric phase of $KNbO_3$ is found to be a rhombohedral one, in agreement with experimental data, and the magnitude of the atomic displacements along [111] are in reasonable agreement with the measured structure. $KTaO_3$ is found to be paraelectric with the cubic perovskite structure in its ground state. These qualitative results persist over experimental and theoretically determined values of the unit-cell volumes; the quantitative results (atomic displacements, depths of the potential wells) may be subject to further refinement in the *ab initio* calculations incorporating nonlocal corrections. For $KNbO_3$, the validity of the eight-site model has been questioned by tracing the total energy path from lowest-energy tetragonal to lowest-energy rhombohedral structure, and it has been found that the structure with tetragonally displaced Nb atoms actually corresponds to a saddle point of the global total energy surface. However, tetragonal lattice strain stabilizes this structure and lowers the total energy towards that of the rhombohedral phase.

ACKNOWLEDGMENTS

We thank O. K. Andersen and A. I. Liechtenstein for useful discussions. Financial support of the Deutsche Forschungsgemeinschaft (SFB 225, Graduate College) is gratefully acknowledged.

*On leave from Institute of Metal Physics, Russian Academy of Sciences, Yekaterinburg, Russia.
[1]W. Cochran, Adv. Phys. **9**, 387 (1960); **10**, 401 (1961); **18**, 157 (1969).
[2]A. C. Nunes, J. D. Axe, and G. Shirane, Ferroelectrics **2**, 291 (1971).
[3]G. A. Samara, Ferroelectrics **73**, 145 (1987).
[4]R. Comes, M. Lambert, and A. Guinier, Solid State Commun. **6**, 715 (1968).
[5]T. P. Dougherty, G. P. Wiederrecht, K. A. Nelson, M. H. Garret, H. P. Jensen, and C. Warde, Science **258**, 770 (1992).
[6]K.-H. Weyrich and R. Siems, Z. Phys. B **61**, 63 (1985).
[7]K.-H. Weyrich, Ferroelectrics **79**, 65 (1988).
[8]R. E. Cohen and H. Krakauer, Phys. Rev. B **42**, 6416 (1990).
[9]R. E. Cohen, Nature **358**, 136 (1992).
[10]A. I. Liechtenstein, I. I. Mazin, C. O. Rodriguez, O. Jepsen, O. K. Andersen, and M. Methfessel, Phys. Rev. B **44**, 5388 (1991); K. Kunc, R. Zeyher, A. I. Liechtenstein, M. Methfessel, and O. K. Andersen, Solid State Commun. **80**, 325 (1991).
[11]R. Resta, M. Posternak, and A. Baldereshi, Phys. Rev. Lett. **70**, 1010 (1993).
[12]A. W. Hewat, J. Phys. C **6**, 2559 (1973).
[13]G. Shirane, H. Danner, A. Pavlovic, and R. Pepinsky, Phys. Rev. **93**, 672 (1954).
[14]M. Methfessel, Phys. Rev. B **38**, 1537 (1988).
[15]M. Methfessel, C. O. Rodriguez, and O. K. Andersen, Phys. Rev. B **40**, 2009 (1989).
[16]U. Schönberger, O. K. Andersen, and M. Methfessel, Acta Metall. Mater. Suppl. **40**, S1 (1992).
[17]T. Neumann, G. Borstel, C. Scharfschwerdt, and M. Neumann, Phys. Rev. B **46**, 10 623 (1992).
[18]P. Blaha, D. J. Singh, P. I. Sorantin, and K. Schwarz, Phys. Rev. B **46**, 1321 (1992).
[19]G. Shirane, R. Newnham, and R. Pepinsky, Phys. Rev. **96**, 581 (1954).
[20]S. R. Andrews, J. Phys. C **18**, 1357 (1985).
[21]E. Wiesendanger, Ferroelectrics **6**, 263 (1974).
[22]S. Yu. Savrasov and A. V. Postnikov (private communication).
[23]U. Hiromoto and T. Sakudo, J. Phys. Soc. Jpn. **38**, 183 (1975).
[24]*Ferroelectrics and Related Substances,* edited by K.-H. Hellwege and A. M. Hellwege, Landolt-Börnstein, New Series, Group III, Vol. 16, Pt. 2 (Springer-Verlag, Berlin, 1981).
[25]G. A. Samara and B. Morosin, Phys. Rev. B **8**, 1256 (1973).